# The Effelsberg Holography Campaign - 2001

M.Kesteven, D.Graham, E.Fürst, O.Lochner & J.Neidhöfer

October 11, 2001

## 1 Introduction

A interesting phase-coherent holography technique was developed as part of the holography campaign to study the Effelsberg 100m antenna. Two high quality images were obtained in May-June, 2001, one during daytime hours, the second at night.

The two images are in good agreement with the earlier Misell-algorithm study, and show the extensive progress made in remedying the outer three rings of panels. The images also show evidence for thermal deformations of the panels.

Section 2 describes the observations; we show that the two images are of excellent quality, with aperture plane resolution of about 1 m, and measurement accuracy better than 0.1mm.

Section 3 assesses the images in order to derive a table of panel setting adjustments.

## 2 The Observations

### 2.1 Overview

The essence of the experiment is to measure the voltage beam pattern of the target antenna.

Two antennas are required for the operation - the target antenna (the Effelsberg 100m, in this instance), and a reference antenna whose role is to provide a phase reference signal. Both antennas observe a strong distant transmitter. For this experiment we used the 11.7 GHz beacon on EutelSat-W2. The reference antenna points towards the satellite for the entire experiment; the target antenna executes a raster map centred on the satellite.

The raster data provide a detailed sampling of the beam pattern; its fourier transform is the field distribution over the aperture plane. The phase distribution is the factor of interest - it can be translated to a surface map; and alignment errors have specific phase signatures which can be identified in the map.

The two antenna signals (from target and reference antennas) are processed in some form of vector voltmeter - to obtain the phase difference and the amplitude ratio. The instrument of choice for this is a cross-correlator. In this experiment we used the Bonn Mk4 correlator - which added the complexity of VLB tape recording as an intermediate step. However, this choice has the virtue of flexibility - the reference antenna can in principle be any distance from the target antenna (eg, at a different observatory).

## 2.2 Setup

The reference antenna is a 1.2m satellite dish located on the control building, about 200 m from the main antenna. Both antennas have good room temperature receivers (Tsys $\sim$ 80 K). Both are equipped with quality low phase noise down converters. The reference antenna has an IF of 995.004 MHz, suitable for the VLBA terminal.

The 100m signal is presented to the mk4 terminal at a frequency of 150 MHz.

The two IFs were offset by 120 hz in order to have a useful fringe rate at the correlator.

In both cases the signal was bandpass filtered - 10 MHz at the receivers, 2.5 MHz in the control room (for data archiving) and 1 MHz at the VLB terminals.

Dynamic range is a serious issue in this experiment - the signal strength is many times Tsys when the 100m antenna points directly at the satellite. We therefore recorded a second, low sensitivity channel from the 100m; this had an effective Tsys of $\sim$ 28000 K. We use the high sensitivity channel for all the beam pattern, except for about a dozen points around the boresight, for which we use the low sensitivity data.

For calibration we use four panels with offsets $\pm$3 mm (ring 7, 9 and 13).

## 2.3 The Satellite

We used EutelSat W2 which is seen, at Effelsberg, at azimuth 168 degrees, elevation 32 degrees.

The beacon frequency is 11.7 GHz, with 9 dBW EIRP. It sits in a narrow hole, $\sim$ 10 MHz wide, in the EutelSat spectrum. A 10 MHz bandpass filter therefore provides a stable environment, independent of the satellite traffic.

The beacon drifted by a few KHz over the course of the experiment.

Eutelsat provided us with very precise satellite ephemerides: the offsets found in our hourly pointing checks were all small. This precision is a serious matter for the holography process, as our imaging is predicated on precise registration of the visibilities on a sky grid centred on the satellite. The EutelSat ephemerides, together with the Effelsberg ability to lock the telescope's coordinate frame to a moving target kept the registration accurate to within a few arcseconds.

## 2.4 The Data

The data are collected from a sequence of elevation scans, with 48 arcsec azimuth separation between scans; a boresight calibration preceding each scan.

This separation is the Nyquist interval (for observations at 11.7 GHz) of an aperture plane function which is band-limited to 110m.

The scan rate was 48 arcsec/second. We sample the data stream (at the Mk4 correlator) every 0.5 seconds.

This observing pattern has quite a high overhead at Effelsberg: there is a 30 second setup period prior to each step, which means that a full map consisting of 133 scans, each 133*48 arcsecs long, should take about 7 hours to complete (133 secs/scan drive time + 30 sec/scan setup + 30 sec/cal setup).

The VLB machinery adds a further penalty: data taking must stop every 44 minutes when the tapes reverse direction.

The circumstances of the two maps are summarised in table 1

| date | start | end | raster size | weather | ID |
|---|---|---|---|---|---|
| 29 May | 9:50 UT | 15:50 UT | 110 scans | light cloud, T=20C | DAY |
| 12 June | 19:20 UT | 3:40 UT | 133 scans | very clear, T∼10C | NIGHT |

Table 1: The observation log

## 2.5 Data Processing

The major processing steps are :

1. Correlate the two tapes in the Mk4 correlator. This produces a file of time-stamped correlation coefficients normalised to unit system temperature.
2. Apply the VanVleck corrections; scale to the observed system temperature; use the time-stamped telescope data to attach to each visibility the azimuth and elevation offsets from the satellite position. Fourier transform each visibility to the spectral domain; extract the two spectral channels with the beacon signal.
3. Calibrate the data (using the boresight observations)
4. Grid the visibilities in the 2-D (az/el) grid. Fourier transform to the aperture plane.
5. Split the complex aperture plane distribution into an amplitude map (the illumination function), and phase (the surface error map).
6. Process the surface error map: correct for pointing, feed offsets; transform from the aperture plane to the reflector surface.

The software details are discussed in the document "Effelsberg_Holography_software", available on request.

## 2.6 Calibration

Every scan was bracketed by boresight calibrations. We use a linear interpolation from these to obtain an amplitude and phase correction for each point on the scan.

The boresight observations therefore give us an indication of the data quality. Figures 1 and 2 show the calibration data for each map. Both are excellent.

The phase/time trends are dominated by the satellite motion, seen with an East-West interferometer of $\sim$ 200m baseline. (The satellite movement was $\sim$ 0.05 degrees in azimuth over the course of the observation).

## 2.7 Signal to Noise

The signal to noise is very high in this experiment:

- Two excellent receivers with system temperatures of 65 K (the 100m) and 85 K (the reference antenna).

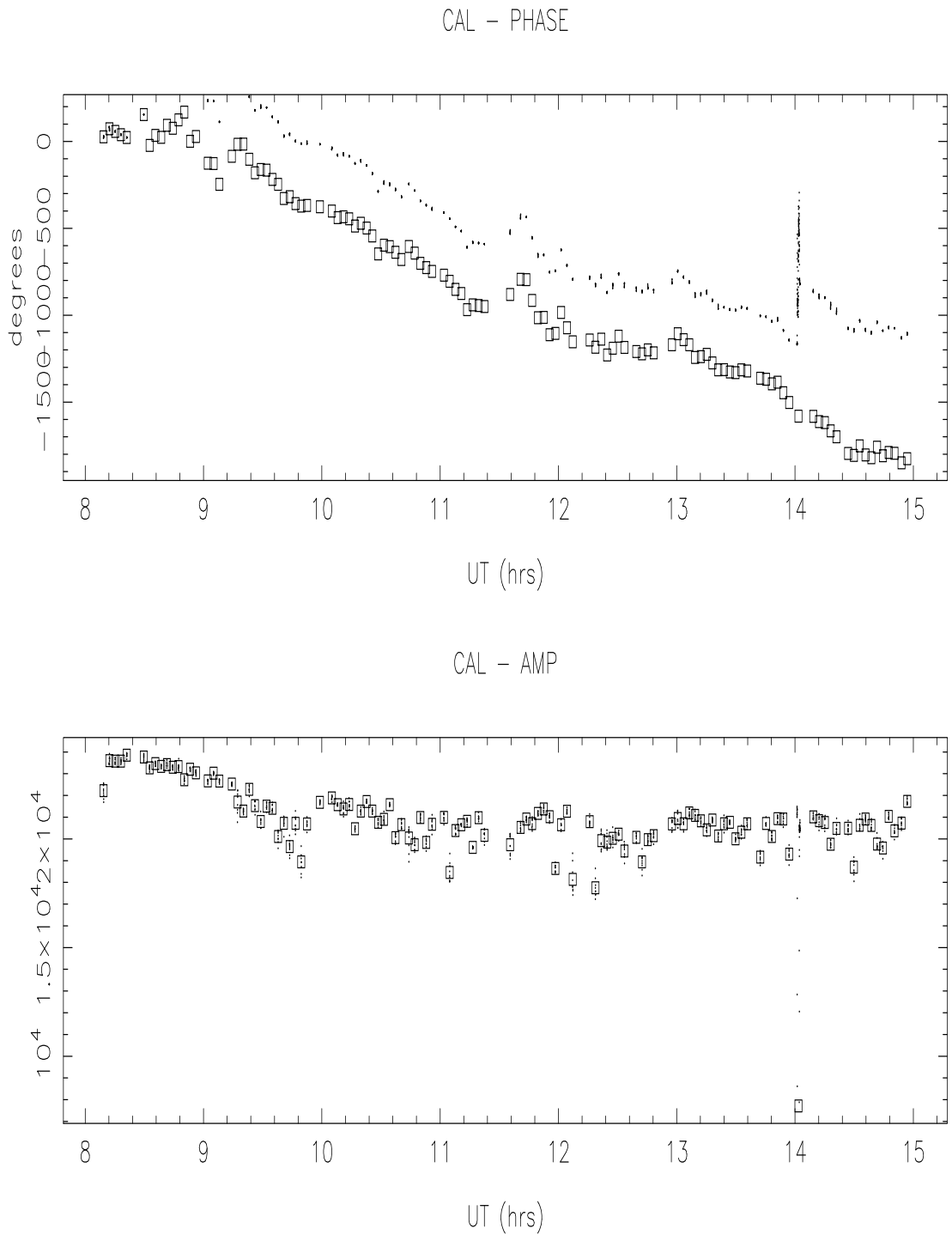


Figure 1: Calibration data from the boresight calibrations of the May 29 run. The large excursions around 14:00 UT are due to a focus check

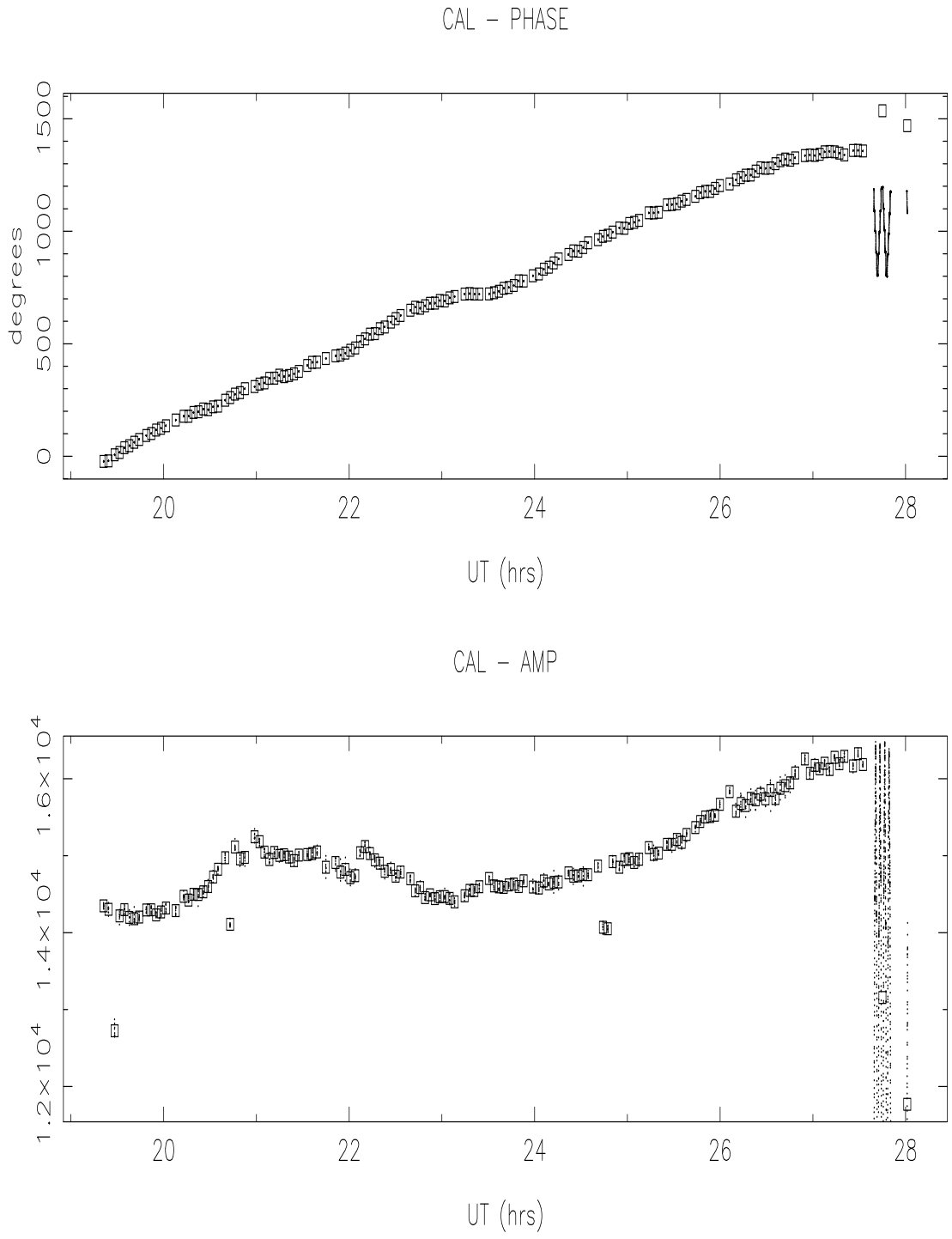


Figure 2: June 12 calibration. The large phase excursions near 28:00 UT are due to focus checks

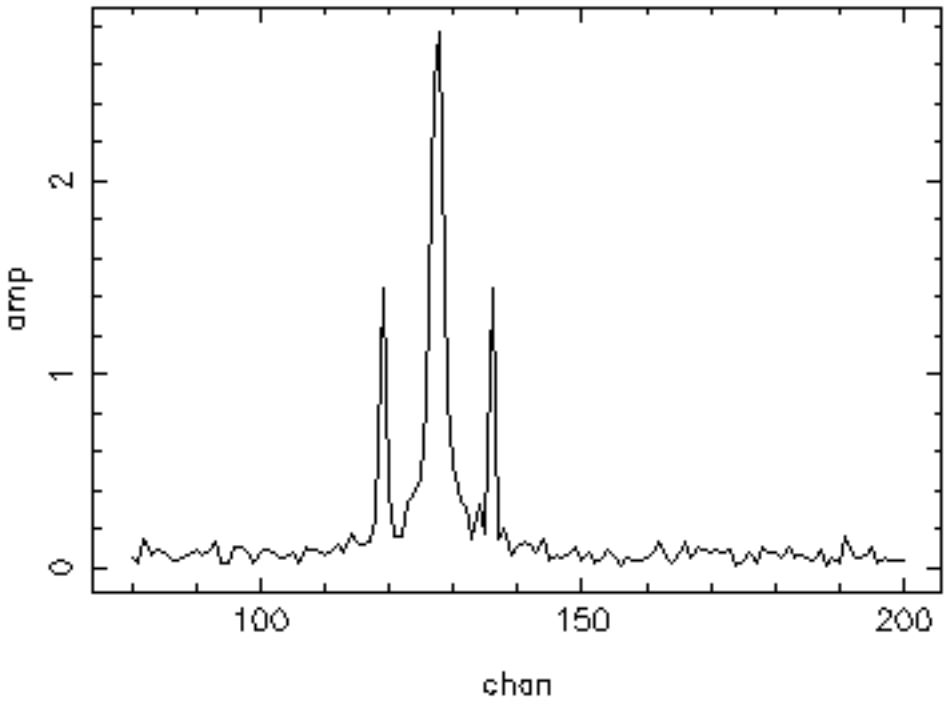


Figure 3: The spectrum of a random visibility somewhere near the edge of the beam map (about 1 degree from boresight) that illustrates the high signal-to-noise of the data

- The satellite signal is confined to two correlator spectral channels (2*2 KHz).
- The beacon is rated at 9 dBW EIRP. The on-line signal monitor with a 2.5 MHz bandpass showed on boresight a level 30 dB above the system temperature.

  At the edge of the map (1.2 degrees from boresight) the signal to noise in the 4 KHz channel visibility is around 20:1, as figure 3 makes clear.

Figure 4 shows the calibrated data (amplitude) in the form of a ruled surface; the horizontal axis is the scan direction (elevation); the scans are stacked in azimuth order. The main features are attributed to :

- The support legs which produce the strong vertical and horizontal sidelobes;

- The central blockage and subreflector which produce the circular sidelobes on the 0.2 degree scale.

The sharp eye will note that the first and last scans were repeated - that is, even at the edges of the map there is little noise in the data. This quality is shown in greater detail in figure 5, which shows a point-by-point comparison of the amplitude and phase for the two copies of the last scan. For reference, the peak (boresight) amplitude is $\sim 10000$.

## 2.8 Accuracy of the Surface Measurements

Studies of the holography procedure, Scott and Ryle (1977), Kesteven (1994), Butler (1999) have shown that the main factors which define the rms surface accuracy are:

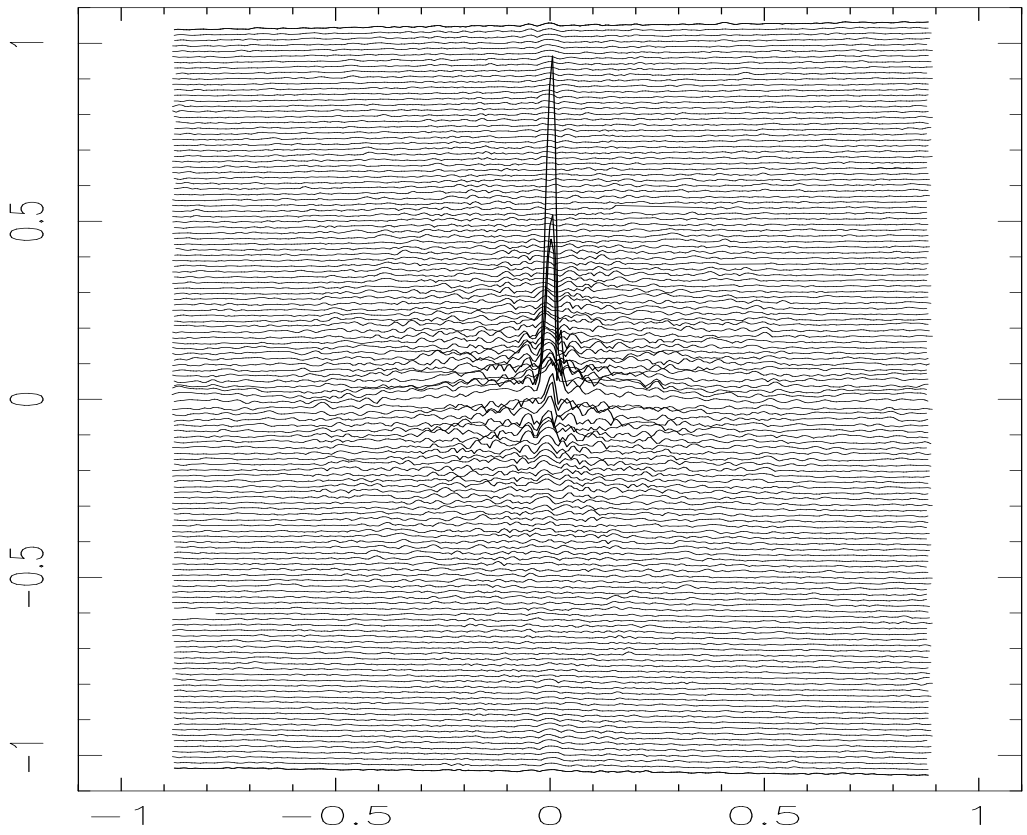


Figure 4: A ruled surface representation of the calibrated data. Each trace is a scan in elevation; the scans are stacked in azimuth order along the vertical axis. This is the NIGHT observation.

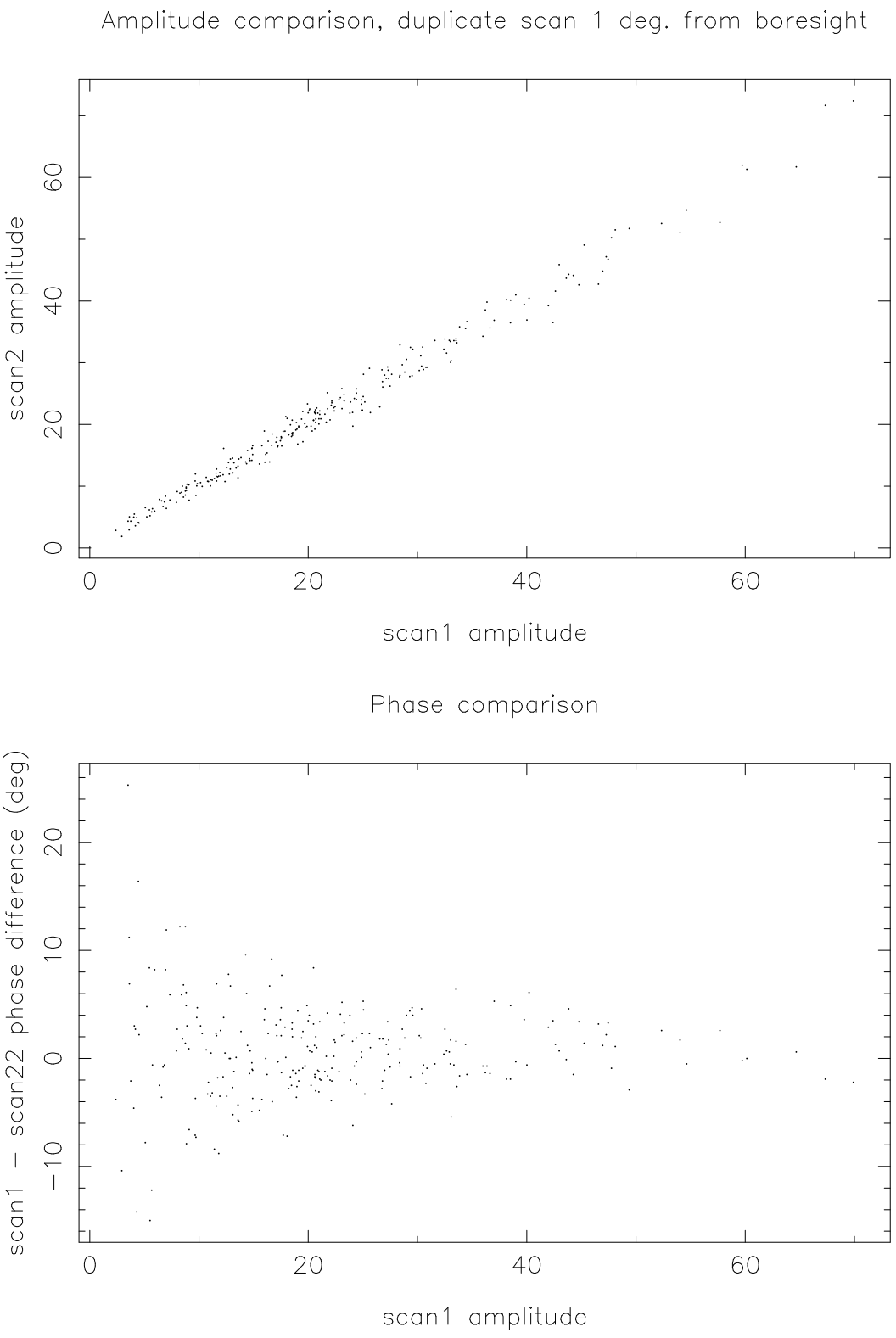


Figure 5: A detailed look at the data quality - the scan most distant from the boresight was repeated. These two figures show the repeatability of the amplitude and the phase.

- **System Noise**

  The rule of thumb is :

  $$\sigma \sim \frac{\lambda N}{3\pi SNR}$$

  for an N by N map, with a boresight signal to noise of SNR.

  We can etimate SNR from figure 5 which shows the phase rms as a function of the visibility amplitude.

  $\sigma_{phase} \sim 5$ (degrees) at Vis = 10.0, which implies a noise amplitude of 0.6 units (rms). The boresight SNR is thus:

  $$SNR = 10000/0.6 \sim 15000.$$

  implying a surface rms of 0.02 mm. We need to refine this estimate, and account for the variation of the illumination over the aperture - in effect, the signal-to-noise is rather worse at the edge of the antenna.

  The complex holography images, after the FFT and the normalisation, will have a pixel noise rms, $\sigma = 0.0005$ (surface current units). Since the illumination falls from 1.0 at the origin to $\sim 0.1$ at the edge, the phase which we map to a surface error will have an rms error of 0.3 degrees at the antenna edge. This means a surface measurement error of 0.04mm (rms).

- **Pointing Errors**

  Random pointing offsets amount to random errors in the gridding operation, and lead to a surface error:

  $$\sigma \sim \frac{\theta_{rms} D}{12}$$

  We derive $\theta_{rms} < 3$ arcsecs from the hourly pointing checks, indicating a contribution to the surface error of

  $$\sigma < 0.1mm$$

  The hourly checks show a systematic trend in the pointing, suggesting a small error in the satellite ephemerides. This could be accommodated at the gridding stage, although it has not been done in this experiment. Our estimate for the pointing rms is also close to the repeatability error in the pointing checks.

- **Phase Errors**

  We rely on the boresight calibrations to provide the fundamental phase reference. Errors in that calibration translate directly to surface error :

  $$\sigma = \frac{\sigma_{phase} \lambda}{12\pi}$$

  We estimate $\sigma_{phase} < 5$ degrees from the calibration plots and the duplicate scans; this translates to :

  $$\sigma < 0.05mm$$

All this suggests that the surface accuracy is $\sim 0.1$mm, set primarily by the antenna tracking and the satellite ephemerides accuracy.

Detailed examination of the two images suggests that this estimate is realistic over most of the antenna, but much caution is required at the outer edges - the error in rings 16 and 17 does appear to be somewhat higher.

### 2.9 Scaling Error

The VLB tape recording path does add an additional source of error, the scaling of the surface error. In conventional holography processing the scale factor is set simply by the wavelength, and so there is no problem.

However, VLB system uses 1-bit sampling, which means that all amplitude is contained in the system temperature data, along with the additional problems which arise when non-gaussian signals are presented to the sampler and correlator. If uncorrected, we obtain a map which is honest in a relative way: the surface error maps are correct in their morphology, but will have an incorrect scale. This is the reason for our cautious approach of recording two IF streams from the 100m - the low sensitivity channel is entirely honest in the region of the boresight; the high sensitivity channel is honest outside the immediate vicinity of the boresight.

### 2.10 Resolution

The resolution in the aperture plane is set by the sampling extent in the visibility plane - 133 scans at 48 arcsec spacing, each scan 133*48 arcsec long.

This translates to a surface resolution of 0.8m.

## 3 Analysis

### 3.1 The Illumination Function

The aperture plane amplitude image is shown in figure 6. This is the night-time image; the daytime image is very little different.

Three factors dominate the amplitude image:

- The feed pattern.

  This should be a smooth, azimuthally symmetric function, falling to low values at the edge of the antenna. Figure 7 shows the radial illumination function computed by averaging the amplitude image around concentric annuli. The predicted function for a feed with a 12 dB taper at the 50m radius is also shown, and is in good agreement.

- The blockage shadows, and their associated Gibbs echoes.

- Phase gradients.

  Our aperture plane distribution is the true distribution convolved with the transform of the sampling window - in effect, the vector average over a patch, roughly 1 $m^2$ in size. Phase variations within the patch will therefore show up as amplitude variations, even if though the amplitude (set by the reflectivity of the panel) has not changed. This is very evident in the haloes surrounding the four calibration panels.

  In addition to the panels however, there are the signatures of a number of other phase gradients in the amplitude map - a number of rings which coincide with the panel rings - ring 14 in particular. These are examined in more detail in the surface error maps.

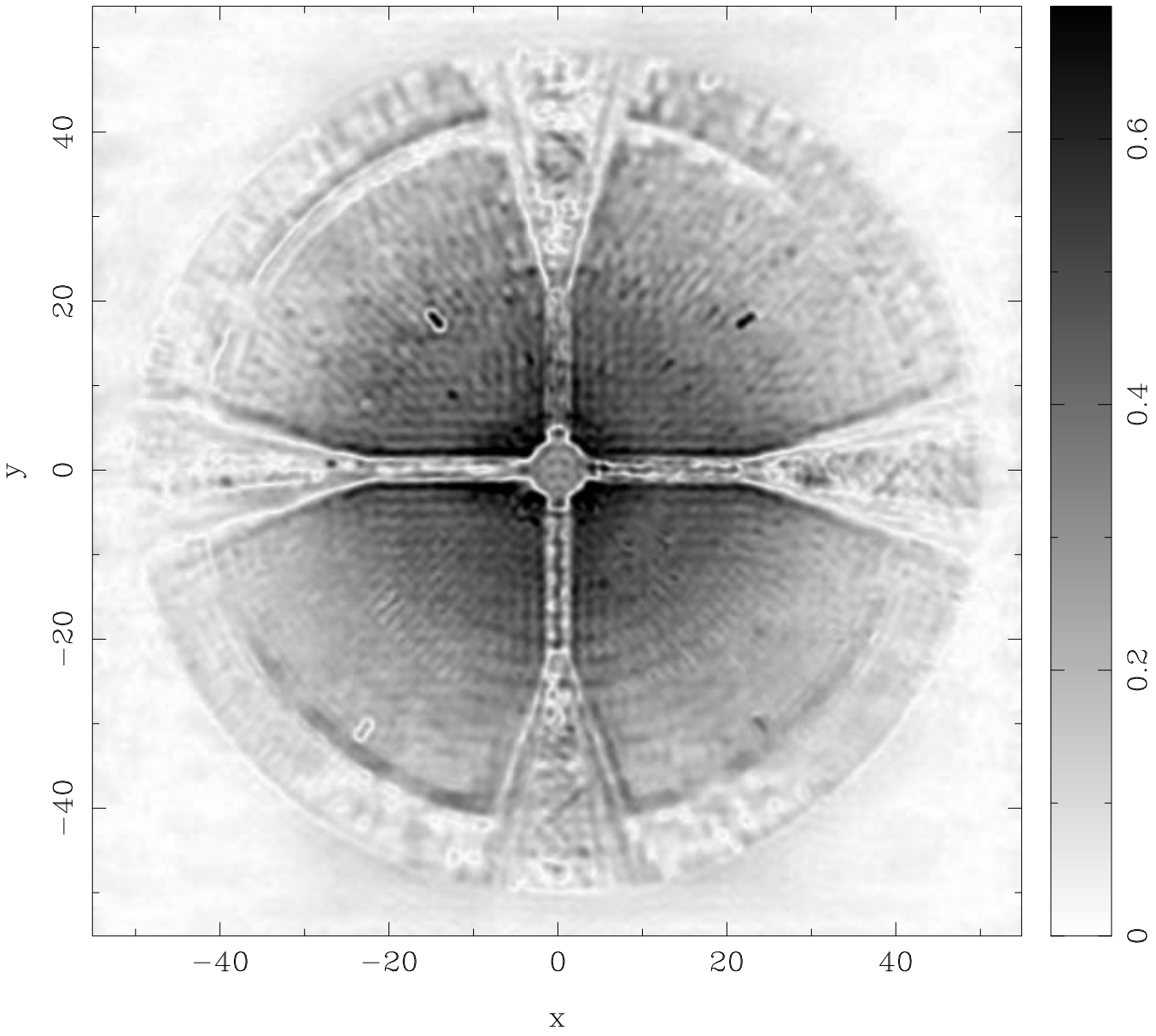


NONE, NONE = 0.00000000E+00, 0.00000000E+00 at pixel (257.00, 257.00)
Spatial region : 1,1 to 512,512
Pixel map image: ../data/june12.V_AMP  Min/max=$8.508\times10^{-5}$/1  Range = 0 to 0.7 (lin)

Figure 6: The aperture plane illumination function, from the June 12 observation

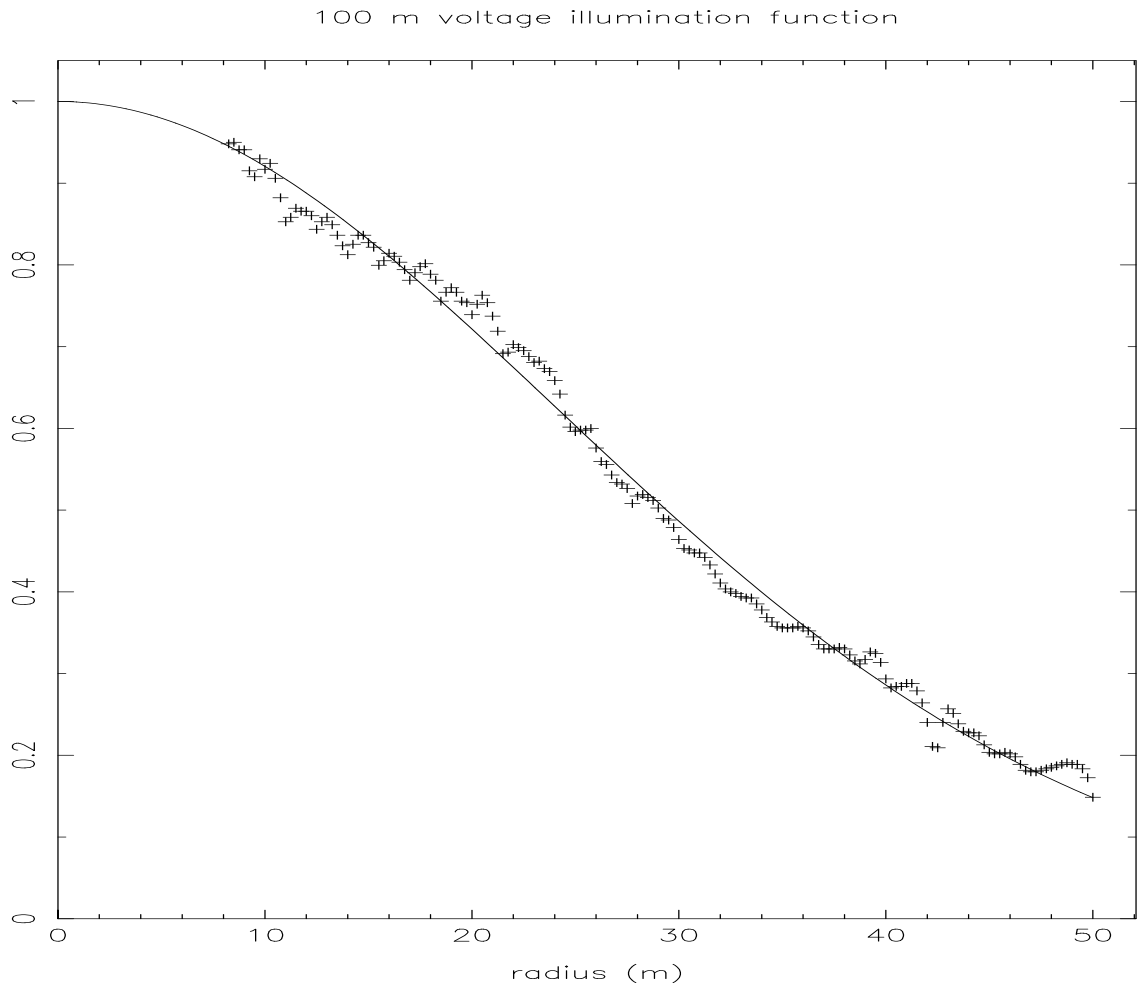


Figure 7: The azimuthally-averaged radial illumination function. The solid line is the function predicted for a feed whose taper is 12 dB at the edge of the antenna (r=50m)

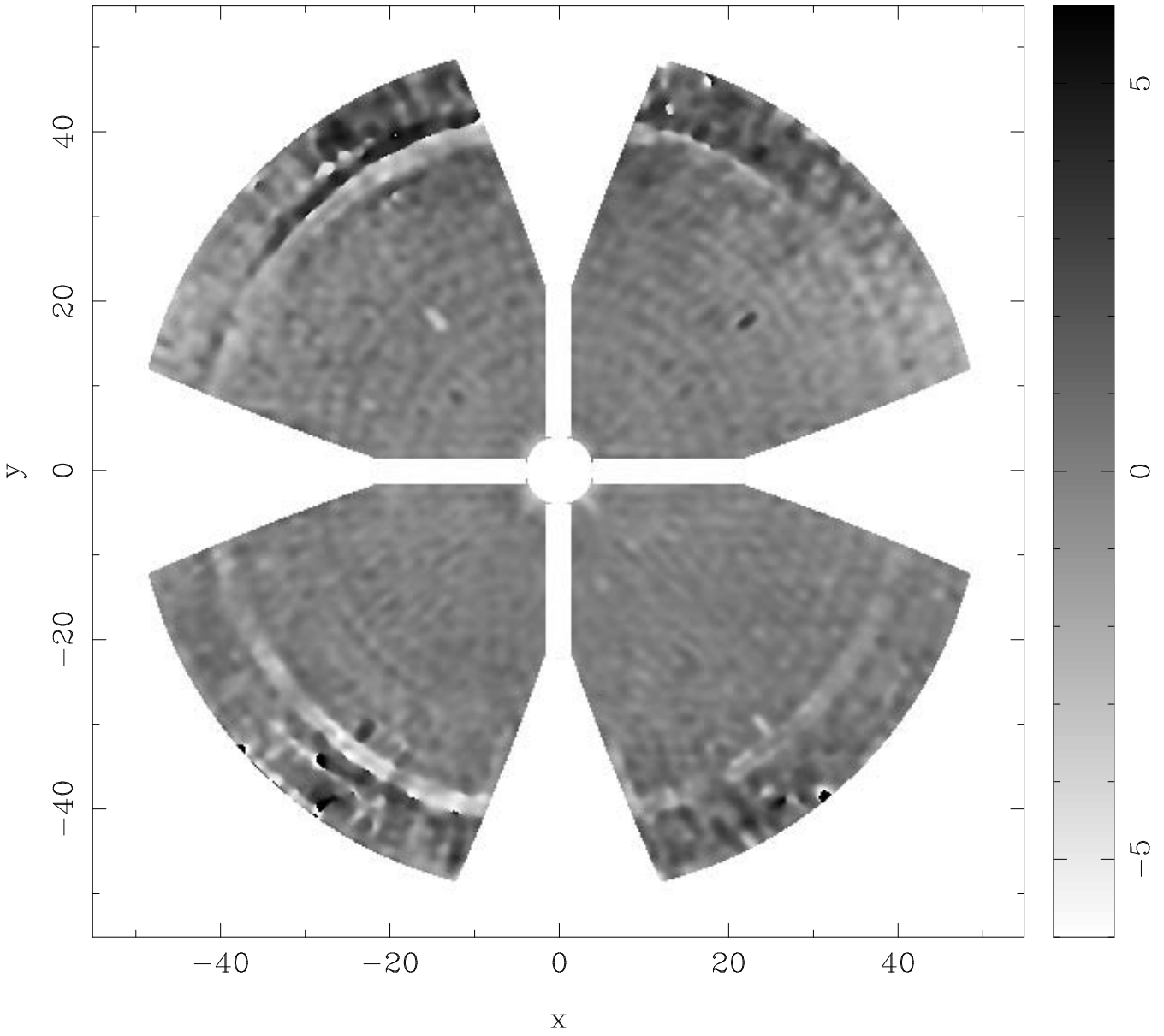


NONE, NONE = 0.00000000E+00, 0.00000000E+00 at pixel (257.00, 257.00)
Spatial region : 1,1 to 512,512
Pixel map image: ../data/may29.V_DEVmm  Min/max=−10.75/10.55  Range = −6 to 6 (lin)

Figure 8: The surface error distribution for the May29 (day) observation

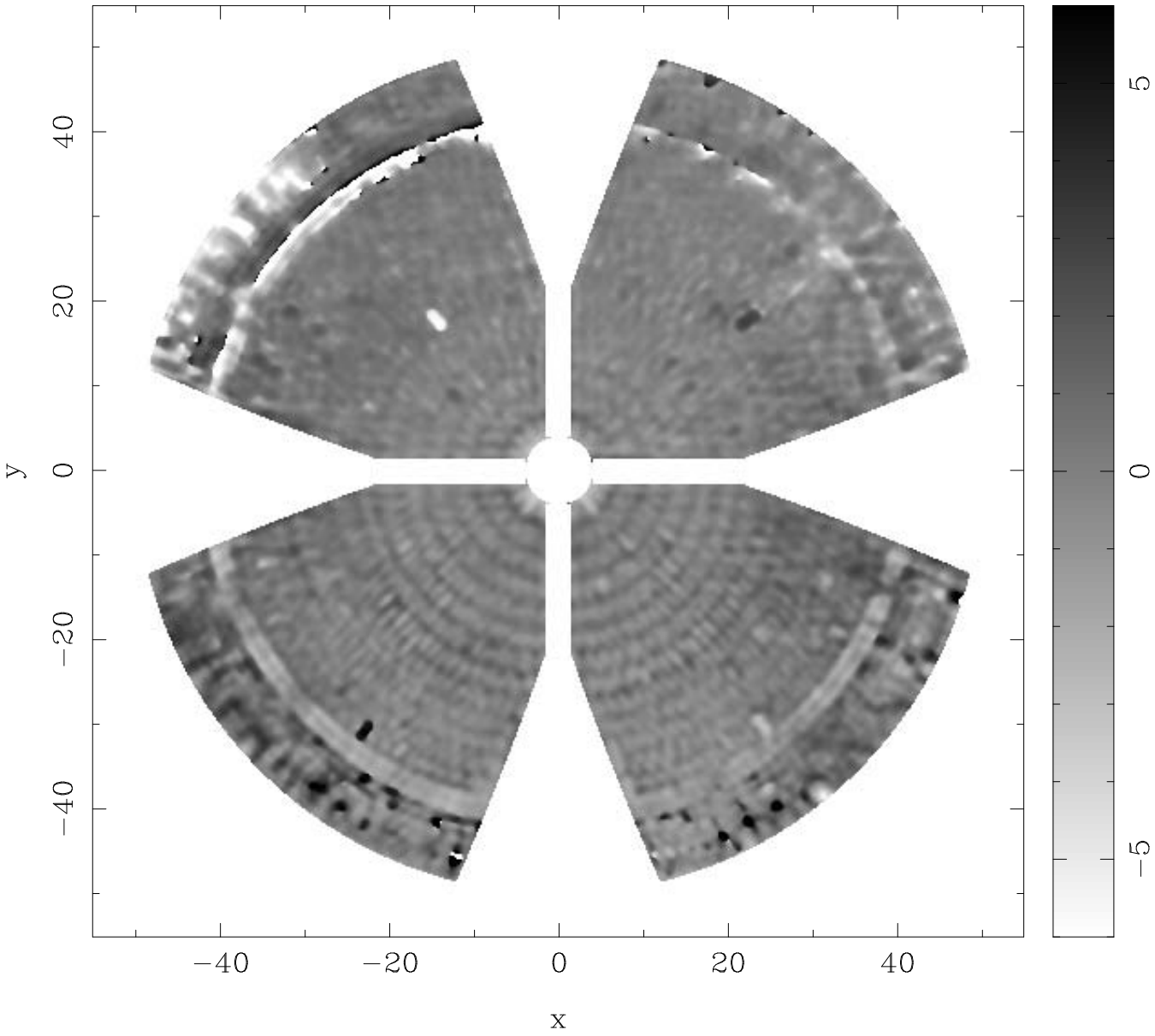


NONE, NONE = 0.00000000E+00, 0.00000000E+00 at pixel (257.00, 257.00)
Spatial region : 1,1 to 512,512
Pixel map image: ../data/june12.V_DEVmm Min/max=−9.873/9.345 Range = −6 to 6 (lin)

Figure 9: The surface error distribution for the June 12 (night) observation

### 3.2 Surface Error maps

The DAY and the NIGHT images are shown in figures 8 and 9. The two images are in general agreement, and confirm that the adjustments already undertaken following the earlier Misell algorithm holography (Reich & Fürst, 1997) have made substantial improvements to the surface.

In the next section we address the issues:

- how much is believable?

- what are the recommended panel setting adjustments?

## 4 Discussion

### 4.1 Data Quality

The two images agree in three areas:

- The central region (out to ring 14) where the surface is well adjusted. Figure 10 is the trace along the panel boundary between rings 6 and 7, clockwise from the dish high-point, from the DAY and NIGHT images. The pixel/pixel correspondance is excellent.

- Ring 14 stands out as a problem; it is depressed by 1 to 1.5 mm over most of the antenna, probably more in the top left quadrant (sectors 1-6).

  In the first three quadrants (clockwise from the top) ring 14 is depressed by about 1.5 mm. In the last quadrant the depression is larger. Visual inspection of the area near az=-45 degrees showed a step of 6 mm between rings 14 and 15; and 2 mm between rings 13 and 14, in excellent agreement with the images. An abrupt transition of this magnitude will produce Gibbs effect ripples in the phase, as is observed.

- The outer rings (15-17) have substantially higher rms than the inner section.

  Here again the top left hand quadrant is worst affected. A scan in azimuth, averaging rings 16 and 17 (figure 11) indicates a step of several mm near az = -45 degrees.

The two images disagree in two areas:

- In the central region (rings 1-13) there are a number of circular local extrema which align with the ring boundaries. These are maxima in the NIGHT image, and minima in the DAY image. This point is shown more clearly in figures 12 and 13 where we have computed the azimuthal average over a number of annuli concentric with the map centre. The panel boundaries are shown as dotted lines. It is clear that the panel mid-points are raised above the panel edges during the day, and lowered at night.

  The rms error contributed by this effect is $\sigma \sim 0.25mm$.

  It is also clear that the radial profile defined by the panel boundaries is the same for both DAY and NIGHT images to within 0.1mm (rms). The profiles defined by the panel mid-points differ by 0.5mm.

  There is a natural explanation for this panel movement: it is thermal in origin, due to the differential expansion between the aluminium panels and the steel backup structure. (See, eg, Christiansen and Hogbom, 1985, p. 52).

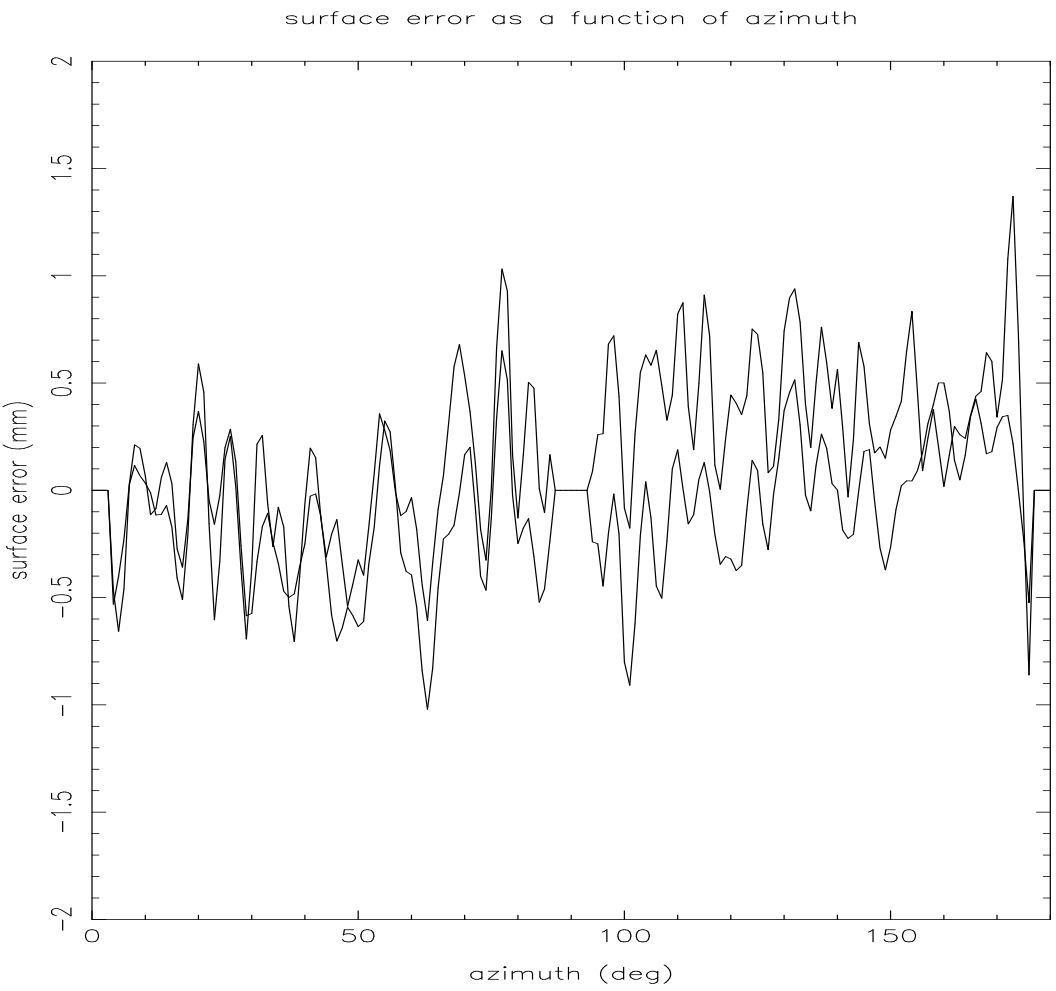


Figure 10: A comparison of a portion the DAY and NIGHT data from the inner part of the reflector. This is the scan along the boundary between rings 6 and 7. AZ=0 is the high point of the dish.

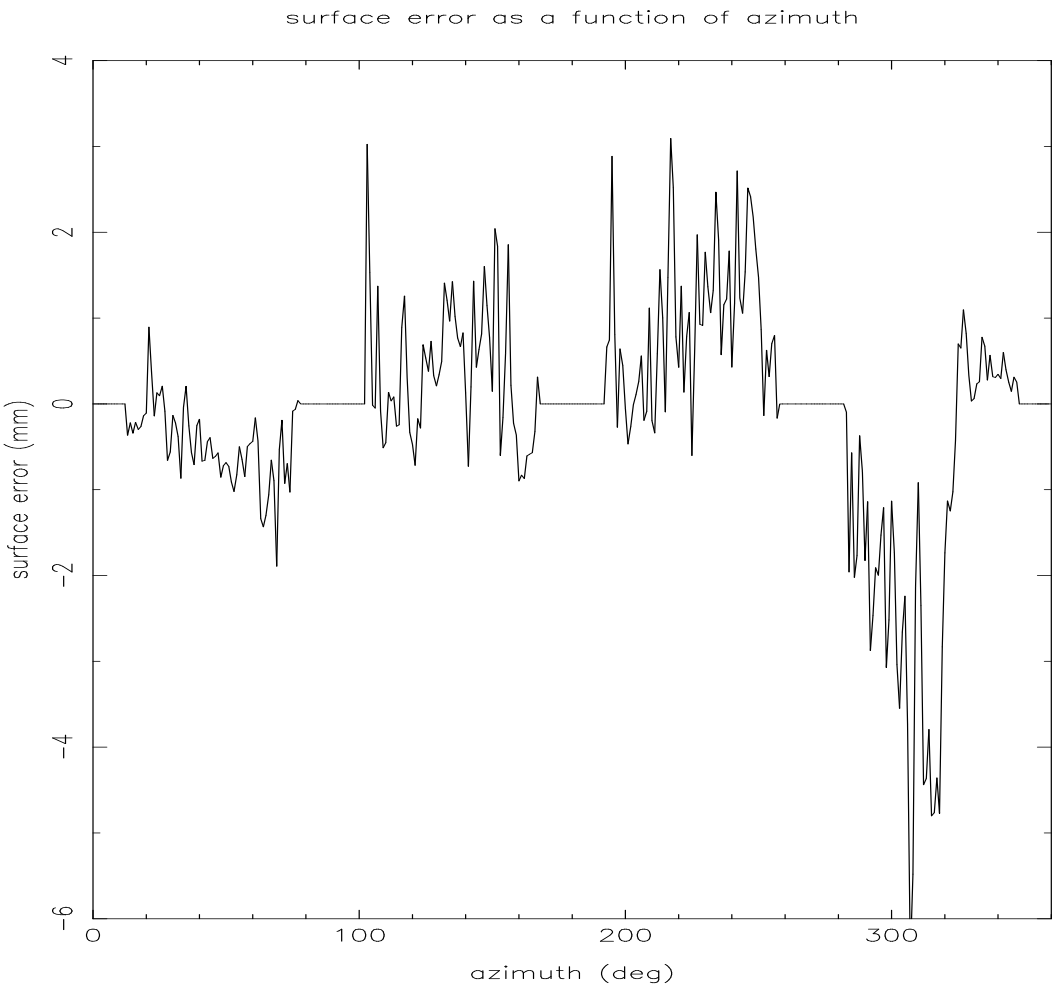


Figure 11: This is a scan around the antenna surface, averaging the surface error of the outer two rings.

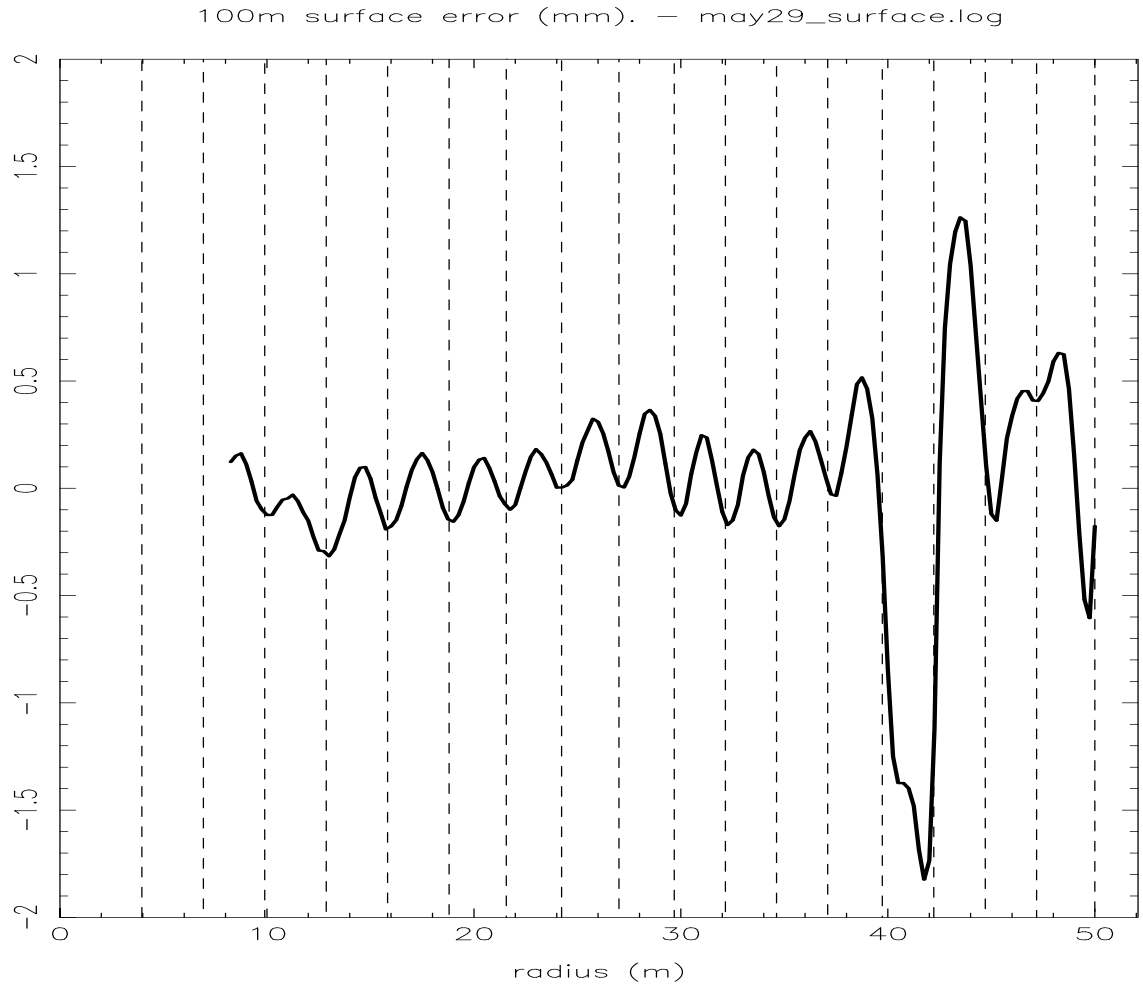


Figure 12: The azimuthally-averaged surface error radial profile for the May29 (day) observation. The vertical dotted lines mark the panel boundaries. Note that the panel mid-points are all higher than the panel edges

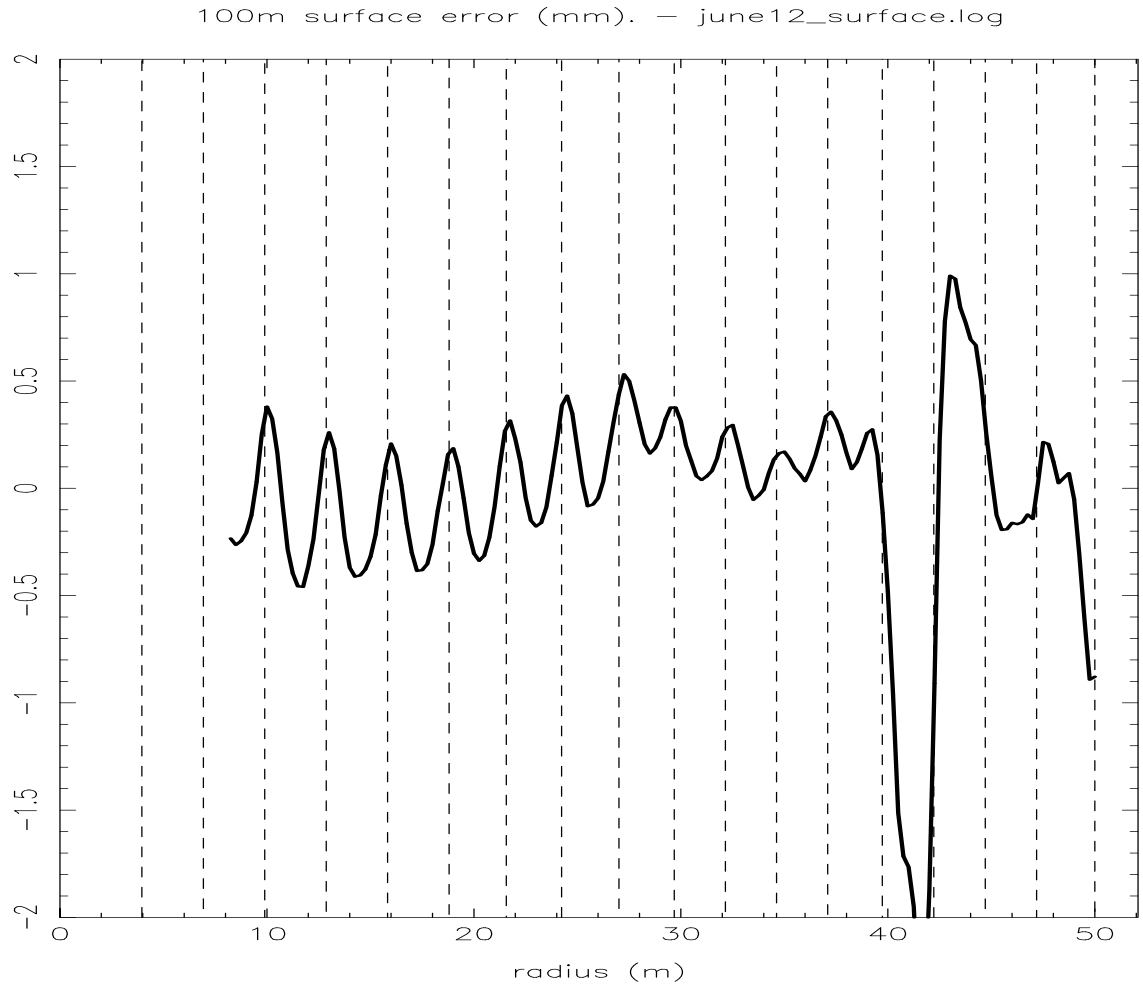


Figure 13: The azimuthally-averaged surface error radial profile for the June12 (night) observation. The vertical dotted lines mark the panel boundaries. Note that the panel mid-points are all lower than the panel edges

If this thermal hypothesis is confirmed, then one might expect the effect to have a zero-point defined at the time the panel is locked to its mounting studs. This could imply that the surface could be optimised for night-time (low temperature) operation.

- There is a large scale deformation of the surface, very roughly astigmatic in appearance in the DAY image, with the top and bottom sections are raised relative to the mean surface. At night there is a smaller effect aligned along the elevation axis.

  It is not clear whether this is a genuine mechanical effect (the surface really is deformed), or an artefact of the analysis. However, the better quality of the calibrations, as well as the cleaner apprearance of the NIGHT amplitude image suggest that the NIGHT image should be used as the basis for the panel adjustment settings.

  The panel-to-panel displacements are little affected by these deformations - that is to say, one can still make meaningful statements about the panels once the deformations are recognised. Great caution is nonetheless advisable.

### 4.2 Surface Rms

The surface error is fairly constant in the central region, but rises sharply in the outer section. Figure 14 shows the rms as a function of radius.

The average, 0.5mm, is higher than the currently accepted value - it may reflect a calibration error in these images; or it may reflect the trend to higher rms as the holography resolution increases. (0.5 mm would suggest a Ruze degradation of 50 % at a wavelength of 7.5mm).

### 4.3 Feed Position

The holography program does an explicit search for the signatures of misalignment errors - feed offsets in this case. The results are given in table 2.

| ID | rms (mm) | $\Delta x$ (mm) | $\Delta y$ (mm) | $\Delta z$ (mm) |
|---|---|---|---|---|
| DAY | 0.68 | 2.9 | -10.0 | 1.7 |
| NIGHT | 0.79 | -2.4 | -9.2 | 0.6 |

Table 2: Results from the surface error fitting program. $\Delta x$ is the feed offset in the focal plane, parallel to the elevation axis; $\Delta y$ is in the focal plane, normal to the elevation axis; and $\Delta z$ is the axial focussing error

The feed offsets are formally significant; however, caution is advisable at this stage - the algorithm could be influenced by the large ring 14 errors in one quadrant. The $\Delta y$ offset, if real, is large enough to cause a loss in efficiency.

## 5 Recommendations

1. **The Thermal Characteristics of the Panels**

   The DAY-NIGHT panel movement should be clarified. It is likely to be a straightforward task with modern laser metrology. It is important to know if the effect is real; and if so, whether the effect could be mitigated by careful choice of the time/temperature when the panels are locked to the backup structure.

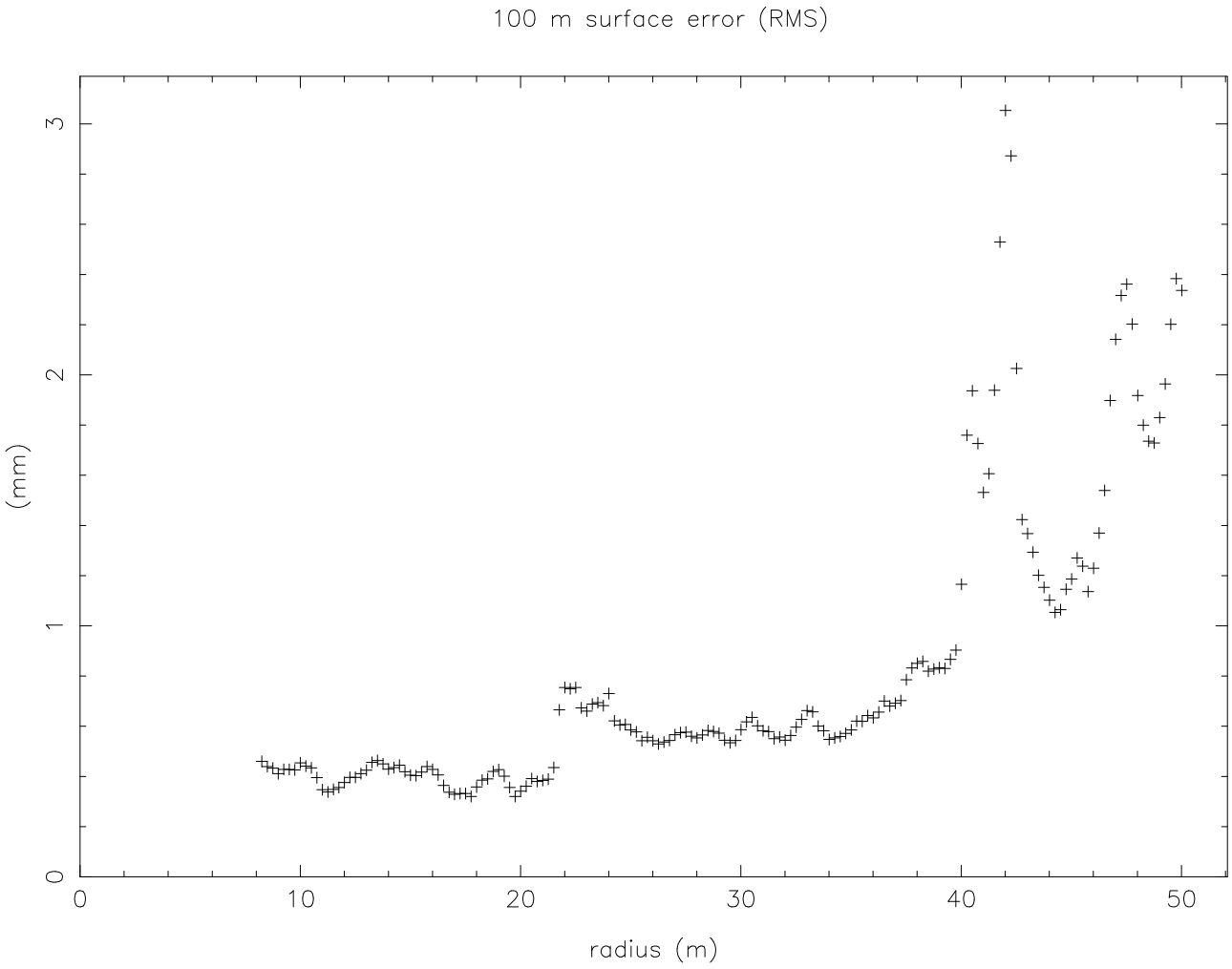


Figure 14: The radial distribution in the surface error rms. The peak near 22-24 m radius is due to the calibration panels of ring 7 and 9

2. **The Thermal Characteristics of the Reflector**

   The apparent large diurnal deformations is also an important question, but probably a‘ harder task to resolve. It is probable that this falls into the collection of known daytime problems, along with pointing shifts and changes in focal length.

3. **Ring 14**

   This ring, (and most importantly the top left hand quadrant) should be raised, at least to form a smooth continuum with rings 13 and 15.

4. **Rings 15, 16 and 17**

   These also need attention, but it might be best to attend to just the top left hand quadrant in the first instance, and wait for fresh holography surveys once the major defects have been remedied.

5. **Better Signal to Noise for the Outer Rings**

   It would be useful if more energy could be collected from the outer rings - Since the satellite provides plenty of signal, a low efficiency feed with wider beam angle could be tolerated.

6. **Minor Housekeeping in rings 1-13**

   Close examination of the images of the central area (rings 1-13) show that a number of panels could benefit from minor adjustment.

7. **Feed Offsets**

   These should be checked after the worst of the ring 14 steps have been remedied.

# 6 References


Butler, B. (1999) VLBA Test Memo N0. 62

Christiansen, W. and Hogbom, J. (1985) Radio Telescopes. CUP (2nd ed).

Kesteven, M. (1994) JEEE (Aus) **14**, 85

Reich, W. and Fürst, E. (1997) MPIfR Technischer Bericht, Nr. 79

Scott, P. and Ryle, M. (1977) MNRAS **178**, 539